International Journal of Power Electronics and Drive System (IJPEDS)
Vol. 17, No. 4, December 2026, pp. 2474~2485
ISSN: 2088-8694, DOI: 10.11591/ijpeds.v17.i4.pp2474-2485

Transient finite-element co-optimization of an asymmetric stator slot-pitch three-phase 12/10 SRM for electric vehicle powertrains

Mohd Zulsyazwan Allan[1], Mohd Luqman Mohd Jamil[1,2], Jenn Hwai Leong[3]
[1]EV-PRODRIVES Research Group, Faculty of Electrical Technology and Engineering, Universiti Teknikal Malaysia Melaka, Melaka, Malaysia
[2]Department of Electrical Engineering, Faculty of Electrical Technology and Engineering, Universiti Teknikal Malaysia Melaka, Melaka, Malaysia
[3]Faculty of Electrical Engineering and Technology, Universiti Malaysia Perlis, Perlis, Malaysia

Article Info

Article history:

Received Jan 13, 2026
Revised Sep 10, 2026
Accepted Oct 4, 2026

Keywords:

Asymmetric stator pole pitch
Electric vehicle powertrain
Short flux path
Switched reluctance motor
Torque ripple reduction

ABSTRACT

Switched reluctance motors (SRMs) provide a robust, rare-earth-free traction option for electric vehicles, but standard 12/10 configurations suffer from high core losses, direct three-phase incompatibility, and power converter complexity. To overcome these issues, this study proposes an asymmetric three-phase 12/10 SRM featuring alternating 36°/24° stator pole pitches to enable localized short flux paths using a standard 3-phase inverter. Machine dimensions were analytically sized for a 48 V, 471 W drive operating at 3000 rpm using M250-35A electrical steel. A 2D transient finite-element framework co-optimized pole arcs, coil turns, and dynamic switching angles. Electromagnetic performance was systematically benchmarked against conventional 6/4, 12/8, 18/12, and standard six-phase 12/10 topologies. The optimized 12/10 SRM delivers 1.57 Nm rated torque while suppressing torque ripple to 24.7%, outperforming the 6/4 (103.3%) and 6-phase 12/10 (26.1%) baselines. Shortened localized flux paths reduce core losses to 6.5 W, an 80% reduction compared to previous baselines, yielding 91.8% efficiency and 0.072 Nm/A torque-per-ampere at 21.4 A phase RMS current. This configuration halves the required power switches and mitigates driveline vibration, delivering a cost-effective, mechanically robust traction solution for electric vehicles.

This is an open access article under the CC BY-SA license.

Corresponding Author:

Mohd Luqman Mohd Jamil
EV-PRODRIVES Research Group, Faculty of Electrical Technology and Engineering
Universiti Teknikal Malaysia Melaka
Hang Tuah Jaya, Durian Tunggal, Melaka 76100, Malaysia
Email: luqman@utem.edu.my

1. INTRODUCTION

The transportation industry is rapidly replacing fossil-fuel drivetrains with electric alternatives to meet the worldwide emissions mandates [1], [2]. Acceleration dynamics, drive-cycle efficiency, and range longevity are directly controlled by the electric traction motor as the primary electromechanical converter in an electric vehicle (EV) powertrain [3], [4]. High starting torque density, broader constant-power speed ratio, high efficiency, and high thermal reliability under intense operating cycles are required in traction drives [5], [6]. Although commercial EVs are dominated by permanent magnet synchronous machines (PMSMs) due to their high-power density, automobile manufacturers are exposed to supply risks, price fluctuations, and extraction concerns through the reliance on rare-earth materials such as neodymium and dysprosium [7], [8].

Furthermore, permanent magnets risk thermal demagnetization under high operating temperatures and heavy armature reaction fields [9]. Therefore, switched reluctance motors (SRMs) have become one of the best candidates to replace these rare-earth-dependent motors [10], [11]. SRM rotors are made entirely of steel laminations without magnets or windings, thus offering high-speed structural robustness, low manufacturing costs, and fault-tolerant capability [12].

Despite the advantages of SRMs such as simpler construction and robustness, SRMs exhibit several electromagnetic trade-offs that have limited their widespread commercial adoption in electric vehicles, such as severe torque ripple during phase commutation caused by the doubly salient geometry and unipolar excitation, which produce non-linear inductance profiles [13], [14]. For example, the 3-phase 6/4 SRMs configuration having a wide stroke angle contributes to fewer strokes per revolution, resulting in excessive torque ripple, which will increase the driveline vibration and acoustic noise [15], [16]. Additionally, increasing the pole arc size to ensure phase overlap increases the unaligned flux leakage to the adjacent poles, thus accelerating the pole-tip saturation and lowering the inductance saliency ratio [17], [18]. Furthermore, conventional 12/10 SRMs designs generate a long flux path topology encircling half of the back iron, increasing the core losses at the same time increase hysteresis and eddy-current losses, reducing the motor efficiency [19]-[21]. Moreover, although standard 6-phase 12/10 SRMs increase their stroke frequency to smooth the torque profile, this motor requires twelve inverter switches, thus increasing the inverter cost due to the increase in power switches and driver packaging volume [22], [23].

To overcome these constraints, previous researchers have explored innovative magnetic topologies and structural modifications such as segmental rotor design, where 12/10 segmental rotor SRMs employ structural modifications by removing their rotor back iron [24], [25]. However, the segmented structure experiences high mechanical stress concentration, high manufacturing complexity, and serious reliability concerns at higher speeds under automotive centrifugal loads [26], [27]. Other than that, implementation of irregular air gaps, stepped poles, and asymmetric pole shoes to modify the motor inductance profile has been investigated in previous studies [28], [29]. Moreover, a short flux path configuration has been introduced by previous studies, where adjacent stator poles with opposing polarities are excited simultaneously, thus confining the magnetic flux to the adjacent teeth without requiring the flux to travel the full circumference to complete its flux path, contributing to lower core losses [19]-[21].

A critical research gap remains in developing an SRM that simultaneously achieves low torque ripple and short flux paths while maintaining its robustness under high-speed operation by using a standard rotor driven by a conventional three-phase inverter:

- Symmetrical 12/10 incompatibility: Standard 12/10 SRMs are unsuitable for direct three-phase operation because the twelve stator poles and ten rotor poles prevent synchronized phase alignment, causing severe phase asymmetry and mutual torque cancellation.
- Segmental rotor limitations: Segmental-rotor designs successfully shorten magnetic flux paths but suffer from high mechanical stress concentrations and compromised structural robustness under high centrifugal forces.
- Suboptimal asymmetric baselines: An earlier asymmetric 3-phase 12/10 design implemented an intermediate 33°/27° slot-pitch distribution. However, this geometry failed to achieve optimal synchronized pole alignment and may cause excessive torque ripple if not properly managed, restricted torque-per-ampere output, and suboptimal core utilization.
- Lack of cross-topology benchmarking: A comparative analysis of the proposed asymmetric three-phase 12/10 SRM against other three-phase SRM topologies such as the conventional 6/4, 12/8, and 18/12 configurations has not yet been comprehensively investigated.

To address these research gaps, this study proposes a 3-phase 12/10 varying stator slot-pitch geometric modification. The primary contributions include:

- Asymmetric slot-pole reconfiguration: Shifting adjacent stator poles by 3° in opposite mechanical directions merges six uniform inductance profiles into three balanced inductance profiles.
- Localized short flux paths: Assigning four stator poles per phase forces flux to close locally across adjacent teeth, reducing active flux path length by one-sixth compared to conventional 12/10 paths while retaining a solid standard rotor.
- Multi-parameter co-optimization: A transient 2D finite element framework co-optimizes stator-rotor pole arcs, coil turns per pole, and dynamic switching angles that satisfy self-starting criteria, tailor phase current rise rates to the narrow conduction window, and ensure full phase demagnetization to avoid excessive torque ripple.

The proposed 3-phase 12/10 varying stator pole pitch has significant theoretical and practical value for EV powertrains, such as lower inverter costs due to the elimination of half of the power switches, gate drivers, and sensors required in the standard 6-phase 12/10 SRM, lessening the back iron saturation and core losses due to the shortened localized flux paths and potentially extending EV battery range during high-speed

cruising. Other than that, increasing the stroke frequency in a high-pole motor configuration such as 12/10 SRM reduces inter-phase torque dips, thus mitigating driveline torsional vibrations, transmission gear rattle, and cabin acoustic noise. Furthermore, the use of standard rotor geometry eliminates the bonding agents required in the segmental rotor configurations, providing high mechanical robustness during high-speed operation. These characteristics show the potential of the proposed design as a cost-effective, efficient, low-noise, and mechanically robust solution for EV powertrains.

2. METHOD

2.1. Switched reluctance motor initial design approach

The initial design of the investigated 3-phase SRMs is established using fundamental analytical sizing formulations, where the stator outer diameter, stack length, air gap, and other geometric specifications and operational constraints, as shown in Table 1, are kept the same to provide a fair electromagnetic performance comparison. The minimum pole arc of the stator, βs must be equal to or larger than the stroke angle, ε, to ensure self-starting capability from any rotor position and minimize unwanted negative torque generation, as in (1), where m is the number of phases, and Nr is the number of rotor poles.

$$\beta_{s_{minimum}} = \frac{2\pi}{mNr} \tag{1}$$

Other than that, the rotor pole arc βr is designed to be slightly larger or almost equal to βs, as in (2).

$$\beta_r \geq \beta_s \tag{2}$$

The βr must be selected carefully, as too large of βr can lessen the saliency ratio due to an increase in unaligned inductance and increase rotor inertia. Therefore, the upper limit of the βr is as in (3), where θfr is the current fall angle at rated operating conditions.

$$\beta_r \leq \beta_s + \theta fr \tag{3}$$

Table 1. Design specifications

Parameter	Ratings	Parameter	Ratings
Output power, P_o	471 W	Inner stator diameter, D_i	62 mm
Output torque, τ_o	1.5 Nm	Inner rotor diameter, D_{sh}	20 mm
Rated speed, N	3000 rpm	Split ratio	0.5
DC voltage, V_s	48 V	Airgap thickness, l_g	1 mm
Axial length, l_a	55 mm	Phase number, m	3
Outer stator diameter, D_o	120 mm	Material type	M250-35A
Outer rotor diameter, D_r	60 mm		

The dimensions of the stator yoke (W_{sy}) and rotor yoke (W_{ry}) are designed to allow and complete the magnetic flux path without driving the back iron into excessive saturation beyond the knee saturation of the electrical steel. Therefore, the stator and rotor yoke are designed to carry approximately half of the total flux ($\frac{\Phi}{2}$) while considering the consumption the iron mass as in (4)-(8), where A_{yoke}, γ_{wsy} and γ_{wry} are the cross-sectional area of the yoke and the per-unit variable for the width of the stator and rotor yoke, respectively.

$$A_{yoke} \geq \frac{\emptyset}{B} \tag{4}$$

$$\gamma_{wsy} = \frac{W_{sy}}{W_{st}} \tag{5}$$

$$0.5 \leq \gamma_{wsy} \leq 1 \tag{6}$$

$$\gamma_{wry} = \frac{W_{ry}}{W_{rt}} \tag{7}$$

$$0.5 \leq \gamma_{wry} \leq 0.8 \tag{8}$$

These analytical formulations control the initial core dimensions and ensure sufficient flux-carrying capacity to minimize excessive saturation while reducing the iron mass consumption and rotor inertia.

2.2. Design of proposed 3-phase 12/10 switched reluctance motor

The conversion of a 6-phase 12/10 SRM into a special 3-phase 12/10 SRM involves not just an electrical reconfiguration of phase windings, but also an alteration in physical stator construction, leading to an entirely new flux path. This proposed 12/10 SRM ensures that the 12/10 SRM is workable for three-phase operation while maintaining balanced electromagnetic performance. The conversion process is based on inductance profile analysis as shown in Figure 1. Initially, they are identical but displaced with a uniform rotor angle of 6° (A-B-C-D-E-F), but later designed with only three uniform profiles left, A'-B'- C'. This configuration mimics a three-phase attribute, representing a three-phase motor system. The A' is obtained by shifting the inductance of Phase A1 to the right by 3° while the inductance of Phase B1 to the left by 3°, resulting in the merging as A'. This process is repeated for other phases of a 6-phase motor, thus resulting in inductances of B' and C' respectively.

The stator teeth of windings A1 and A2 of the same phase are shifted in the opposite direction by 3°, while the corresponding B1 and A2 are shifted in the other direction by an equal distance. As a result, the stator having two different slot pitches, λs1 and λs2 are alternately in sequence around the stator periphery to form a three-phase 12/10 motor. This transformation results a set of four poles associates in each phase excitation that result a shorter flux path. For a conventional 6-phase 12/10 SRM, the magnetic flux flows through the stator poles which are situated about half a circumference away from each other, while the new design results in the flux moving only through two adjacent stator teeth for alignment with rotor poles. The new length of the magnetic path is shortened by one-sixth compared to the conventional 6-phase 12/10 SRM. Figure 2 shows how the design is structurally altered in a linear dimension, and Figure 3 shows the 2-D layout for the proposed motor designs.

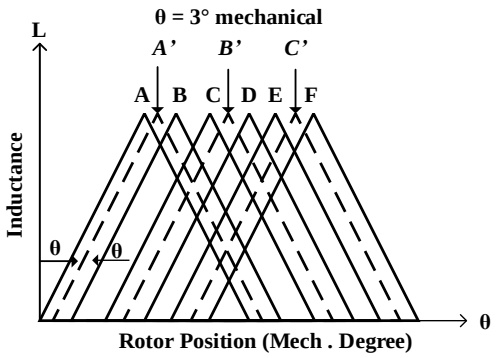

Figure 1. The inductance profile shift in a conventional 12/10 SRM

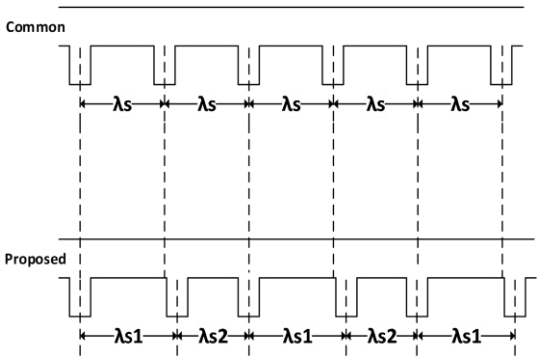

Figure 2. Common and proposed designs of 3-phase 12/10 SRM (λ_s=30°, λ_{s1}=36°, λ_{s2}=24°)

2.3. Optimization approach of 3-phase switched reluctance motor

For optimization purpose, parameters such as influence of pole arcs, Bs and Br, where the Bs is optimized by choosing the stator pole embrace configurations in the range of 0.55 to 0.4 which is large enough and fulfil the self-starting requirement and proven by previous study to produce high average torque and lower torque ripple and followed by Br where the rotor pole embrace were made slightly larger than the Bs approximately by approximately 5% to 10% larger which is enough to increase the average torque while considering the effect of the saliency ratio. Furthermore. The switching angle, TON, and TOFF are parametrically swept by ±0.5°, where the TOFF is initially held fixed, and TON is swept first until the lowest torque ripple, Tripple, is achieved; then the step will repeat for TOFF, where TON is fixed at this optimal angle, and TOFF is swept until the final minimum torque ripple is obtained. This switching angle optimization will reduce the commutation torque dips between inter-phase strokes and prevent unwanted negative torque by ensuring that the phase current is fully demagnetized before entering the negative inductance slope region. Furthermore, the number of turns per pole, NPOLE, has also been optimized by adjusting it to control the phase inductance ($Lph \propto N2$). This NPOLE optimization will control the current rise rate, where a lower NPOLE will increase the current rise rate due to lower inductance, and vice versa. As number of turns optimization is to let the current rise faster or slower where lower number of turns let the current rise and fall faster but higher peak current if not properly manage causing higher copper losses and higher number of turns let the current rise and fall slower but too high number of turns may prevent the motor to reach the optimum current thus fail to achieve the targeted torque. Figure 4 shows the optimization approach flowchart for the 3-phase SRMs.

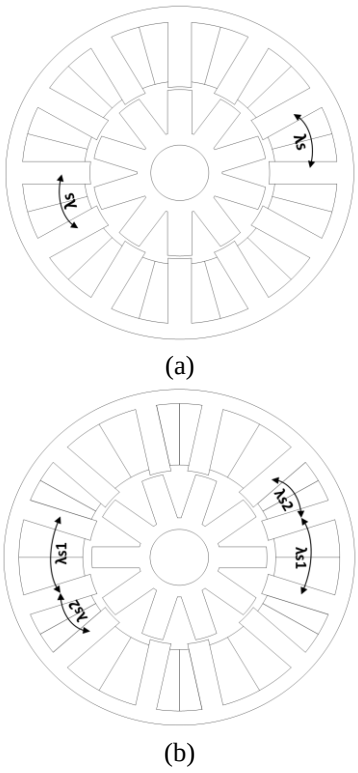

Figure 3. 12/10 designs: (a) conventional 12/10 SRM and (b) proposed 12/10 SRM

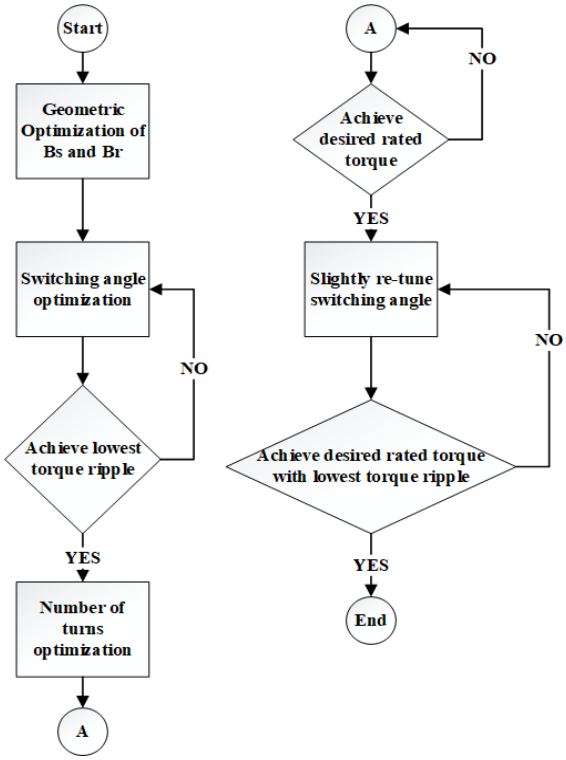

Figure 4. Optimization approach flowchart

2.4. Finite element solver setup

All electromagnetic performance results reported in this study, including output torque, excitation current, flux-linkage and $\varphi - i$ characteristics, were obtained using the finite-element solver in Ansys Maxwell. Figure 5 illustrates the proposed design modelled in the software's 2D transient solver. An adaptive mesh refinement was applied and automatically refined.

The modelling procedures are summarized as follows and illustrated as in Figure 6.

i) Geometric modelling: A 2D planar cross-section of the 3-phase SRMs is generated, defining the precise contours of the stator core, rotor core, non-magnetic shaft, and winding slot geometries.
ii) Material property definition: Non-linear magnetic properties of M250-35A electrical steel are assigned to the stator and rotor laminations to accurately capture non-linear core saturation (B-H curve), while high-conductivity annealed copper is assigned to the coil domains.
iii) Winding configuration and excitation: Coil regions are defined by assigning the exact conductor cross-sections, turn counts per phase, terminal polarities, and excitation current paths corresponding to the proposed switching topology.
iv) Boundary condition assignment: Magnetic vector potential boundaries (Dirichlet boundary, $A_z = 0$) are enforced along the outer periphery of the stator frame to confine the magnetic field within the machine envelope and model zero flux leakage into the ambient surroundings.
v) Mesh discretization: The domain is discretized using finite-element mesh refinement, specifying a maximum element length of 4mm in the winding slots and a refined maximum length of 0.5 mm across high-flux-gradient regions, including the air gap, pole tips, and core teeth, to guarantee numerical convergence.
vi) Solver formulation: A time-stepping transient electromagnetic solver coupled with mechanical rotor motion is implemented as the primary calculation engine to evaluate time-dependent field variations and dynamic rotational performance.
vii) Post-processing analysis: The computed solution fields are post-processed to extract dynamic transient performance (instantaneous torque, current waveforms, and core losses) under 3000 rpm constant speed.

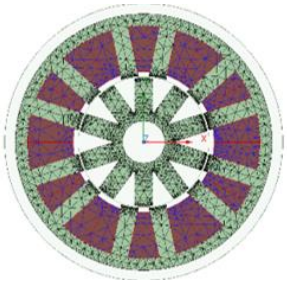

(a)

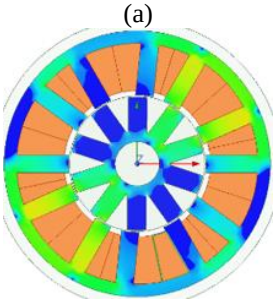

(b)

Figure 5. Proposed design: (a) meshed model and (b) contour of flux density

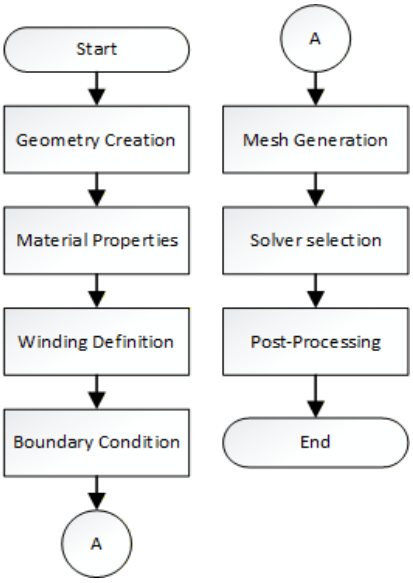

Figure 6. 2D finite element setup flowchart

3. RESULTS AND DISCUSSION

3.1. Optimization and analysis of 3-phase 6/4, 12/8. 18/12 and proposed 12/10 switched reluctance motor

Multi-parameter optimization analysis focusing on the geometric pole arcs, β_s and β_r, winding turns per pole, $N_{pole,}$ and excitation switching angles, T_{on} and T_{off} was performed to increase the electromagnetic performance for all the evaluated design configurations, as tabulated in Table 2. All of the design configurations successfully achieve the targeted rated torque between 1.52 Nm and 1.60 Nm and operate at 3000 rpm constant speed. By narrowing β_s and β_r in the 6/4, unaligned flux leakage can be prevented from entering the adjacent rotor slots, which contributes to a higher saliency ratio, while the T_{on} were advanced so that the motor reaches its peak current before entering the rising inductance $(dL/d\theta > 0)$ thus enhancing the average torque by 24.6%. In higher-pole SRMs such as 18/12 SRMs, the narrow stroke window needs a faster current rise; therefore, N_{pole} is optimized to reduce the phase inductance ($L \propto N_{pole}^2$) to accelerate the current rise rate, thus achieving a 194.5% torque enhancement in the 18/12 SRMs and reducing the torque ripple by 53.2% by optimizing the switching angles. Although it enhances the average torque and reduces the torque ripple, it increases the I_{rms} current stress from 9.3 A to 20.6 A, thus increasing the copper losses (I^2R) and may reduce the efficiency of the electric motor.

Table 2. Initial and optimized numerical values for the evaluated motor designs

Design metric	6/4		12/8		18/12		Proposed 12/10	
	Initial	Optimized	Initial	Optimized	Initial	Optimized	Initial	Optimized
β_r	36°	31.5°	18°	18°	12°	10.5°	15°	15°
β_s	33°	30°	16.5°	16.5°	11°	10°	16.2°	16.2°
N_{pole}	55	65	28	26	26	20	26	21
T_{on}	-10°	-13.5°	-3°	-6°	-3°	-5.2°	-8°	-6.5°
T_{off}	38°	35°	15°	16°	12°	11°	11°	11.5°
T_{ave} (Nm)	1.22	1.52	0.91	1.60	0.52	1.52	0.93	1.57
T_{ripple} (%)	125.9	103.3	52.5	36.3	53.6	25.1	28.4	24.6
I_{rms} (A)	11.4	11.2	11.3	17.3	9.3	20.6	14.8	21.4

In the proposed 12/10 SRMs perspective, maintaining the stator and rotor pole arc while reducing the N_{pole} to achieve the optimum peak current in higher-pole SRMs due to a narrow stroke window and adjusting the switching angle so the optimum peak current can be achieved before entering the positive inductance slope and ensuring complete phase demagnetization before entering the negative inductance slope $(dL/d\theta < 0)$ to eliminate negative torque and minimizing torque ripple contributes to the enhancement of average torque production to 1.57 Nm with the lowest torque ripple by 24.7%, matching the low-ripple profile of high-pole topologies compared to the other evaluated motor designs while operating in a standard 3-phase

inverter. However, the proposed 12/10 SRMs exhibit the highest RMS phase current compared to the other design configurations, showing a current stress trade-off but still can be managed. Figure 7 compares the torque output versus rotor position waveform for the initial and optimized 3-phase switched reluctance motor.

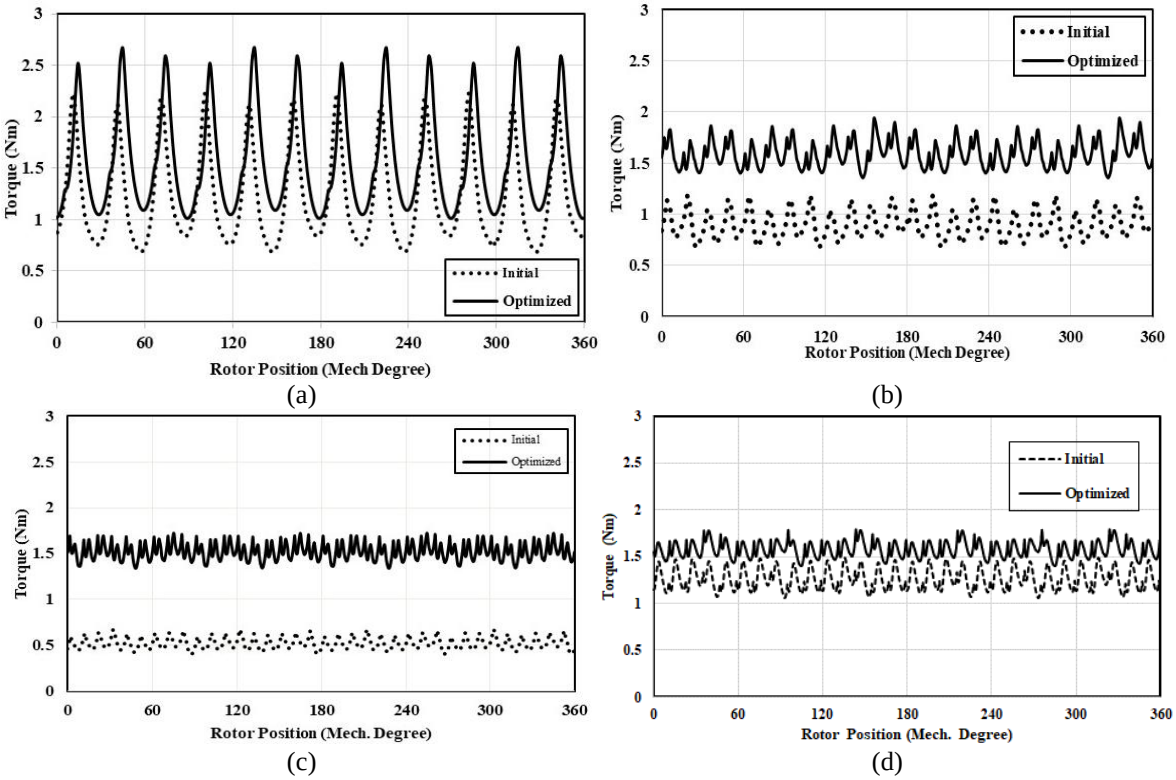

Figure 7. Torque output versus rotor position waveform for initial and optimized 3-phase SRMs: (a) 6/4, (b) 12/8, (c) 18/12, and (d) proposed 12/10

3.2. Comparative electromagnetic performance analysis between optimized 3-phase switched reluctance motor designs

Electromagnetic torque generation is largely controlled by slot-pitch distributions and stator-rotor pole combination as shown in Figure 8. Broad stator pole arcs ($\beta s = 30.0°$) with a stroke angle of $\varepsilon = 30°$ limit the commutation to 12 strokes every mechanical revolution in a 6/4 switched reluctance motor (SRM). As a result, instantaneous phase torque drops sharply during inter-phase transitions, causing significant torque dips that contribute to the excessive torque ripple of 103.3%. On the other hand, higher-pole topologies (12/8 and 18/12) enforce continuous phase overlap by increasing stroke frequencies to 24 and 36 pulses per revolution ($\varepsilon = 15°$ and 10°). By adjusting the slot pitch to $\lambda s1 = 36°$ and $\lambda s2 = 24°$ in the proposed 12/10 SRM, active pole pairs are symmetrically aligned across adjacent phases, creating balanced commutation overlap and lowering torque ripple to 24.7%. This reduction of torque ripple lowers unwanted rotor shaft vibrations and reduces rattling and gear noise. This will increase the transmission durability, reduce shaking during acceleration, and improve overall passenger comfort.

The current waveform illustrated in Figure 9 compares the required excitation current for all of the motor designs to attain the 1.5 Nm rated torque at 3000 rpm constant speed. In the 6/4 SRMs, the longer conduction period permits more winding turns, resulting in a lower I_{rms} of 11.2 A due to higher phase inductance and a slower current rise caused by higher winding turns to attain the desired torque. Other than that, a higher pole number such as 18/12 and the proposed 12/10 SRMs exhibit a shorter conduction period. This shorter conduction period needs a faster current rise within the available excitation interval to attain the desired torque at 3000 rpm; thus, fewer windings are applied to reduce the phase inductance. This results in steeper and sharper current pulse waveforms, giving a higher I_{rms} value of 20.6 A and 21.4 A, respectively. This higher RMS current increases the copper losses, imposing more thermal and electrical requirements on the motor and power converter. Consequently, the winding, semiconductor devices, insulation system, and cooling setup must be suitably designed to ensure reliable operation under these increased current requirements.

Figure 10 compares the flux-linkage waveforms among the investigated SRMs topologies. The 6/4 SRM reach the highest peak value of flux-linkage and exhibits the widest flux linkage profile due to the higher winding turns and wider pole arcs which increase the phase inductance and induce core saturation at lower currents. The 18/12 and proposed 12/10 SRMs exhibits the lowest flux linkage due to lower winding turns. This reduction in flux linkage value is due to the narrower pole arcs and modified stator pole pitch overlap, which may lower the aligned phase inductance. Although the proposed 12/10 SRMs exhibit the lowest flux linkage values, this reduction of flux linkage may reduce the magnetic loading and effectively suppress the back-EMF at 3000 rpm. For an EV powertrain, this reduced flux swing lowers back-EMF at 3000 rpm, delays magnetic saturation knee-points to enhance overload torque capability, and lowers back-iron core losses to preserve battery energy during highway cruising.

Figure 11 compares the $\varphi - i$ energy conversion loop among the investigated SRM topologies. The 6/4 SRMs exhibit the largest enclosed area per stroke with a steep trajectory contributing to the highest energy conversion per stroke due to the higher winding turns, which produces a higher peak MMF. Although achieve the largest enclosed area, it will contribute to higher local core saturation at lower phase currents due to this elevated MMF. Other than that, the other SRMs topologies shows a progressively flatter profiles compared where the 18/12 and proposed 12/10 SRMs show the smallest area due to its fewer winding turns, which restrict the operating MMF and limit the peak flux linkage. Although they achieve the smallest enclosed area, their higher stroke frequency compensates for the reduced energy per stroke thus sustaining the desired average torque while preventing excessive magnetic loading in each phase. In EVs applications, distributing electromechanical conversion across higher-frequency strokes significantly lowers the torque ripple, reduces mechanical driveline vibrations and overall improves comfort in EV traction applications.

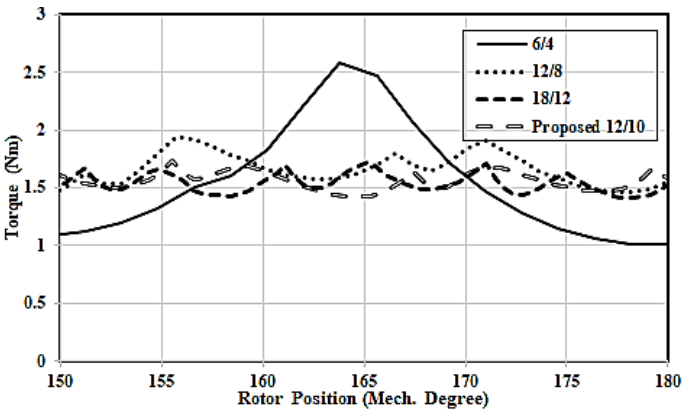

Figure 8. Enlarged torque output versus rotor position waveform in 3-phase motors

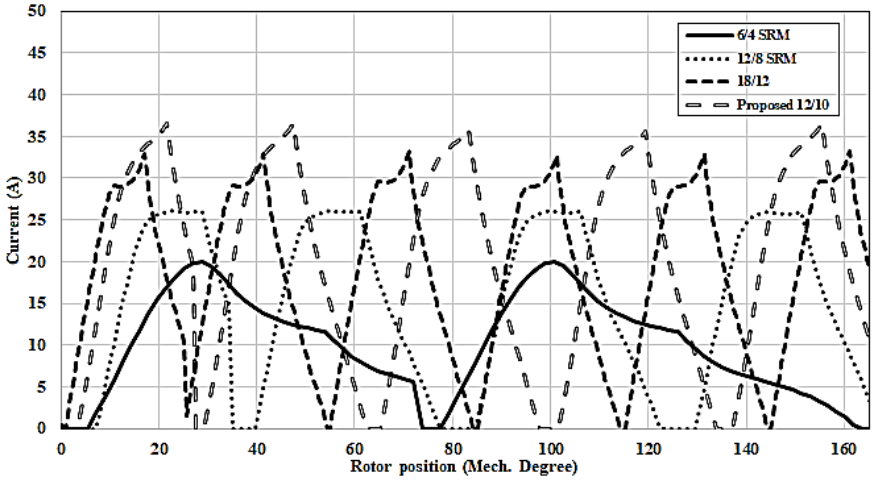

Figure 9. Enlarged current phase A waveforms versus rotor position waveform in 3-phase motors

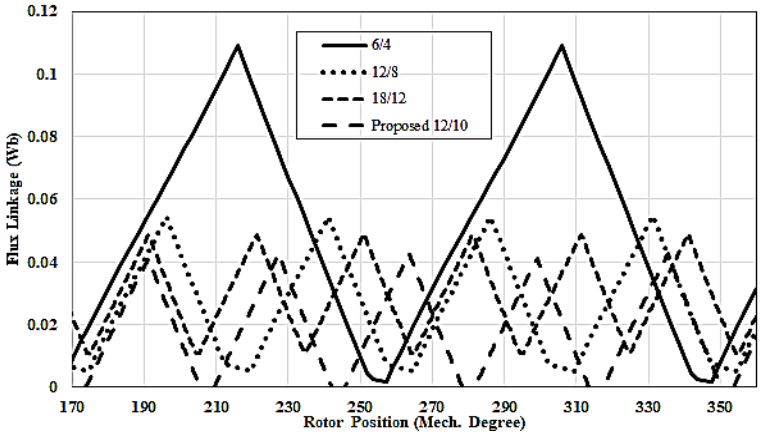

Figure 10. Enlarged phase A flux linkage versus rotor position for 3-phase motors

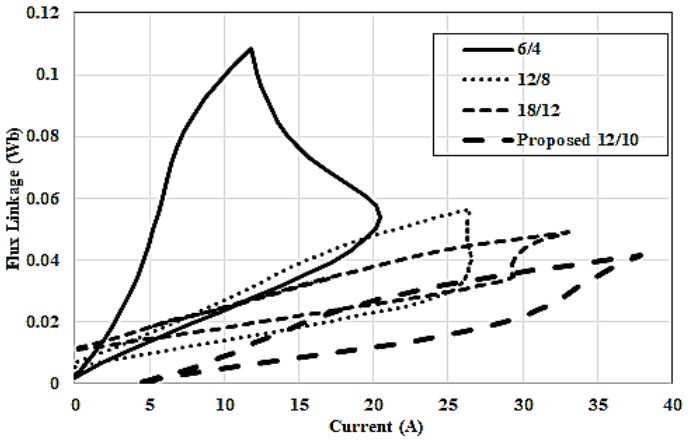

Figure 11. Phase A $\varphi - i$ characteristic in 3-phase motors

3.3. Performance comparison with published benchmark SRM topologies

The previous 12/10 SRMs and 6-phase 12/10 SRMs were redesigned with identical dimensions with the proposed 12/10 but with different in switching angles due to the differences in the stator slot pitch that affecting the inductance profile, to achieve same 1.5 Nm rated torque under 3000 rpm constant speed for fair comparison. Table 3 summarizes the performance comparison among all the 12/10 SRMs. The proposed 12/10 SRM reaches an overall efficiency of 91.8% and significantly reduces average core losses to 6.5 W while the conventional 6-phase configuration provides the highest torque per ampere (0.106) but results in excessive core losses (35.1 W). In contrast, the proposed 12/10 SRM improves torque-per-ampere by 22% compared to the earlier asymmetric 12/10 design while reducing core losses by 80%. Moreover, each 3-phase asymmetric design introduces a short flux path topology and needs just 6 inverter switches compared to the standard 12/10 6-phase SRMs which require 12 switches and exhibit the greatest torque ripple (26.1%). Therefore, the proposed 12/10 SRMs may be the most suitable option for EV drivetrain where it gives an efficiency of 91.8% which optimally enhances battery driving range and low core losses prevent thermal overheating during prolonged high-speed cruising.

Table 3. 12/10 SRMs performance comparison

Parameter	Proposed 12/10	Previous 12/10	Standard 12/10
No. of phases	3		6
Stator slot pitch	36°/24°	33°/27°	Uniform = 30 °
Inverter switches	6 switches		12 switches
Flux path	Short		Long
Torque per ampere	0.072	0.059	0.106
T_{ripple} (%)	24.7	20.5	26.1
Average core losses (W)	6.5	32.8	35.1
Efficiency (%)	91.8	86.7	88.6

3.4. Flux contour of motor designs at the maximum torque

The 6/4 SRMs exhibits extreme tip saturation with flux density distributions at maximum torque reaching 2.84 T at the stator tip and 2.36 T at the rotor tip. In contrast, pole-tip flux densities in the 12/8 and 18/12 SRMs remain 1.39 T indicating core underutilization. The proposed 12/10 SRM achieves balanced magnetic loading where the peak flux densities at the rotor and stator tips reach 1.50 T and 1.78 T, respectively, operating near the saturation knee of M250-35A electrical steel without entering severe over-saturation while preserving effective flux distribution across the yoke (1.60 T) and stator tooth body (1.34 T). Therefore, the proposed 12/10 may be the best option for EV powertrains, as it reduces magnetic fringing, acoustic noise, and eliminates localized core heating by reducing the high tip over-saturation (>2.3 T) present in the 6/4 SRMs. Other than that, the proposed 12/10 design utilizes its magnetic core more effectively than the 12/8 and 18/12 SRMs to produce the desired 1.5 Nm torque while having identical motor size (Stator outer diameter and axial length). This balanced electromagnetic behavior ensures high drive efficiency, lower thermal stress, and dependable operation across dynamic vehicle cycles. Table 4 summarizes the numerical values of flux density at critical points, and Figure 12 compares the contour map for all the investigated configurations at the maximum torque.

Table 4. Contour map numerical values at critical points

Points	6/4 (T)	12/8 (T)	18/12 (T)	Proposed 12/10 (T)
Rotor tip	2.361	1.197	1.070	1.500
Stator tip	2.841	1.382	1.102	1.780
Stator tooth body	1.069	0.858	1.178	1.347
Rotor tooth body	0.901	0.719	0.509	0.802
Stator yoke	1.047	1.078	1.345	1.608
Rotor yoke	0.860	0.795	0.878	1.110

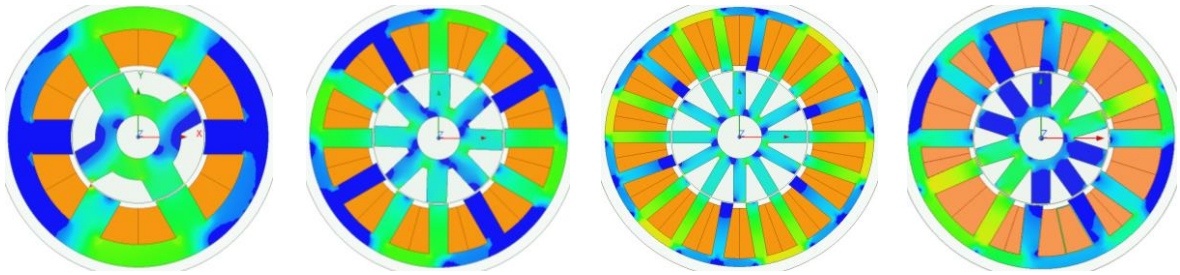

(a) (b) (c) (d)

Figure 12. Flux contour at the maximum torque: (a) 6/4, (b) 12/8, (c) 18/12, and (d) proposed 12/10

4. CONCLUSION

In this study, an asymmetric 3-phase 12/10 SRM design featuring alternating 36°/24° stator pole pitches was developed and optimized using a multi-parameter 2D transient finite-element framework. The proposed design achieved an average rated torque of 1.57 Nm and reduced torque ripple to 24.7%, matching the performance profile of a high-pole machine while reducing converter complexity from a 6-phase to a standard 3-phase inverter. By confining magnetic flux to adjacent stator teeth, the proposed design shortened the active flux path length by one-sixth, reducing core losses and increasing overall efficiency to 91.8%. Despite these advantages, a trade-off is observed in an elevated phase RMS current of 21.4 A resulting from a narrowed conduction window that demands a faster current rise rate, which in turn increases thermal stress on the phase windings and inverter switches. Furthermore, this investigation was restricted to 2D finite-element modelling without accounting for 3D axial end-effects, mechanical vibrations, or thermal limits. To build upon these findings, future work will focus on fabricating a physical prototype for experimental validation, conducting 3D thermal and vibroacoustic analyses, and evaluating dynamic current-profiling strategies across standardized automotive drive cycles.

FUNDING INFORMATION

The authors would like to thank the Ministry of Higher Education (MOHE) for continuous support of research development under the national grant scheme, FRGS/1/2024/TK07/UTEM/02/13, and Universiti Teknikal Malaysia Melaka (UTeM) for providing UTeM BALUMNI Scholarship.

AUTHOR CONTRIBUTIONS STATEMENT

This journal uses the Contributor Roles Taxonomy (CRediT) to recognize individual author contributions, reduce authorship disputes, and facilitate collaboration.

Name of Author	C	M	So	Va	Fo	I	R	D	O	E	Vi	Su	P	Fu
Mohd Zulsyazwan Allan	✓	✓	✓			✓		✓	✓		✓			
Mohd Luqman Mohd Jamil	✓	✓		✓	✓	✓	✓	✓	✓	✓		✓	✓	✓
Jenn Hwai Leong	✓			✓	✓		✓	✓		✓		✓		

C : **C**onceptualization
M : **M**ethodology
So : **So**ftware
Va : **Va**lidation
Fo : **Fo**rmal analysis
I : **I**nvestigation
R : **R**esources
D : **D**ata Curation
O : Writing - **O**riginal Draft
E : Writing - Review & **E**diting
Vi : **Vi**sualization
Su : **Su**pervision
P : **P**roject administration
Fu : **Fu**nding acquisition

CONFLICT OF INTEREST STATEMENT

Authors state no conflict of interest.

DATA AVAILABILITY

The data that support the findings of this study are available from the corresponding author, [MLMJ], upon reasonable request.

REFERENCES

[1] C. Liu, K. T. Chau, C. H. T. Lee, and Z. Song, "A critical review of advanced electric machines and control strategies for electric vehicles," *Proceedings of the IEEE*, vol. 109, no. 6, pp. 1004–1028, Jun. 2021, doi: 10.1109/JPROC.2020.3041417.

[2] C. H. T. Lee, W. Hua, T. Long, C. Jiang, and L. V. Iyer, "A critical review of emerging technologies for electric and hybrid vehicles," *IEEE Open Journal of Vehicular Technology*, vol. 2, pp. 471–485, 2021, doi: 10.1109/OJVT.2021.3138894.

[3] F. Mahmouditabar and N. J. Baker, "Design optimization of induction motors with different stator slot rotor bar combinations considering drive cycle," *Energies*, vol. 17, no. 1, Dec. 2023, doi: 10.3390/en17010154.

[4] Z. Q. Zhu and D. Howe, "Electrical machines and drives for electric, hybrid, and fuel cell vehicles," *Proceedings of the IEEE*, vol. 95, no. 4, pp. 746–765, Apr. 2007, doi: 10.1109/JPROC.2006.892482.

[5] E. Bekiroglu and S. Esmer, "Design and double-stage optimization of synchronous reluctance motor for electric vehicles," *Electric Power Components and Systems*, vol. 51, no. 20, pp. 2557–2572, Dec. 2023, doi: 10.1080/15325008.2023.2240792.

[6] Y. Cheng, L. Ding, T. Zhao, and S. Cui, "Design and optimization of electric vehicle traction motor considering rotor topology and manufacturing uncertainty," *IEEE Transactions on Industrial Electronics*, vol. 71, no. 5, pp. 5034–5044, May 2024, doi: 10.1109/TIE.2023.3288195.

[7] J. D. Widmer, R. Martin, and M. Kimiabeigi, "Electric vehicle traction motors without rare earth magnets," *Sustainable Materials and Technologies*, vol. 3, pp. 7–13, Apr. 2015, doi: 10.1016/j.susmat.2015.02.001.

[8] K. T. Chau, C. C. Chan, and Chunhua Liu, "Overview of permanent-magnet brushless drives for electric and hybrid electric vehicles," *IEEE Transactions on Industrial Electronics*, vol. 55, no. 6, pp. 2246–2257, Jun. 2008, doi: 10.1109/TIE.2008.918403.

[9] Y.-J. Yang, D.-H. Kim, and Y.-M. You, "Demagnetization analysis of interior permanent magnet synchronous motors under realistic vehicle driving conditions," *IEEE Access*, vol. 14, pp. 6501–6513, 2026, doi: 10.1109/ACCESS.2026.3653208.

[10] M. Takeno, A. Chiba, N. Hoshi, S. Ogasawara, M. Takemoto, and M. A. Rahman, "Test results and torque improvement of the 50-kW switched reluctance motor designed for hybrid electric vehicles," *IEEE Transactions on Industry Applications*, vol. 48, no. 4, pp. 1327–1334, Jul. 2012, doi: 10.1109/TIA.2012.2199952.

[11] S. Han, K. Diao, and X. Sun, "Overview of multi-phase switched reluctance motor drives for electric vehicles," *Advances in Mechanical Engineering*, vol. 13, no. 9, Sep. 2021, doi: 10.1177/16878140211045195.

[12] J. Ji, T. Zhang, Z. Xu, and X. Sun, "Overview of position sensorless control for switched reluctance motor drive systems," *Advances in Mechanical Engineering*, vol. 18, no. 7, Jul. 2026, doi: 10.1177/16878132261466545.

[13] K. Diao, X. Sun, G. Lei, Y. Guo, and J. Zhu, "Multiobjective system level optimization method for switched reluctance motor drive systems using finite-element model," *IEEE Transactions on Industrial Electronics*, vol. 67, no. 12, pp. 10055–10064, Dec. 2020, doi: 10.1109/TIE.2019.2962483.

[14] M. A. Aman, W.-J. Chang, M. S. Aslam, M. Salman, and H. Bilal, "Control strategies and power converter topologies for switched reluctance motors in electric vehicle applications: A comprehensive review," *An International Journal of Optimization and Control: Theories & Applications (IJOCTA)*, vol. 15, no. 4, Oct. 2025, doi: 10.36922/IJOCTA025280122.

[15] T.-S. Chuang, "Acoustic noise reduction of a 6/4 SRM drive based on third harmonic real power cancellation and mutual coupling flux enhancement," *Energy Conversion and Management*, vol. 51, no. 3, pp. 546–552, 2010, doi: 10.1016/j.enconman.2009.10.020.

[16] Jian Li, Xueguan Song, and Yunhyun Cho, "Comparison of 12/8 and 6/4 switched reluctance motor: noise and vibration aspects," *IEEE Transactions on Magnetics*, vol. 44, no. 11, pp. 4131–4134, Nov. 2008, doi: 10.1109/TMAG.2008.2002533.

[17] R. Krishnan, *Switched Reluctance Motor Drives*. CRC Press, 2017, doi: 10.1201/9781420041644.

[18] S. E. M. Mohammadi, P. Chen, M. Moallem, B. Fahimi, and M. Kiani, "An alternate rotor geometry for switched reluctance machine with reduced torque ripple," *IEEE Transactions on Energy Conversion*, vol. 38, no. 2, pp. 939–947, Jun. 2023, doi: 10.1109/TEC.2022.3229999.

[19] M. Diko, P. Rafajdus, P. Makys, P. Dubravka, L. Szabo, and M. Ruba, "A novel concept of short-flux path switched reluctance motor for electrical vehicles," *Advances in Electrical and Electronic Engineering*, vol. 13, no. 3, Sep. 2015, doi: 10.15598/aeee.v13i3.1309.

[20] J.-W. Ahn, "Characteristics analysis of short flux-path 4/3 SRM," *Journal of international Conference on Electrical Machines and Systems*, vol. 2, no. 1, pp. 40–44, Mar. 2013, doi: 10.11142/jicems.2013.2.1.40.
[21] P. Lobato, S. Rafael, and A. J. Pires, "Comparison of losses in short flux-path topologies for switched reluctance machines," in *2020 IEEE 14th International Conference on Compatibility, Power Electronics and Power Engineering (CPE-POWERENG)*, Jul. 2020, pp. 255–260, doi: 10.1109/CPE-POWERENG48600.2020.9161661.
[22] W. Qiao, S. Han, K. Diao, and X. Sun, "Optimization design and control of six-phase switched reluctance motor with decoupling winding connections," *Applied Sciences*, vol. 12, no. 17, Sep. 2022, doi: 10.3390/app12178801.
[23] A. Siadatan, E. Afjei, and H. Torkaman, "Analytical design and fem verification of a novel three-phase seven layers switched reluctance motor," *Progress In Electromagnetics Research*, vol. 140, pp. 131–146, 2013, doi: 10.2528/PIER13040705.
[24] J. D. Widmer, R. Martin, and B. C. Mecrow, "Optimization of an 80-kW segmental rotor switched reluctance machine for automotive traction," *IEEE Transactions on Industry Applications*, vol. 51, no. 4, pp. 2990–2999, Jul. 2015, doi: 10.1109/TIA.2015.2405051.
[25] Y. Lan, M. A. Frikha, J. Croonen, Y. Benômar, M. El Baghdadi, and O. Hegazy, "Design optimization of a switched reluctance machine with an improved segmental rotor for electric vehicle applications," *Energies*, vol. 15, no. 16, Aug. 2022, doi: 10.3390/en15165772.
[26] Z. Xu, D.-H. Lee, and J.-W. Ahn, "Comparative analysis of segmental rotor type switched reluctance motors with single teeth winding," in *2015 IEEE Industry Applications Society Annual Meeting*, Oct. 2015, pp. 1–8, doi: 10.1109/IAS.2015.7356744.
[27] Z. Xu, T. Li, F. Zhang, Y. Zhang, D.-H. Lee, and J.-W. Ahn, "A review on segmented switched reluctance motors," *Energies*, vol. 15, no. 23, Dec. 2022, doi: 10.3390/en15239212.
[28] G. F. Lukman and J.-W. Ahn, "Torque ripple reduction of switched reluctance motor with non-uniform air-gap and a rotor hole," *Machines*, vol. 9, no. 12, Dec. 2021, doi: 10.3390/machines9120348.
[29] C. Lee, J. Lee, and I. G. Jang, "Shape optimization-based design investigation of the switched reluctance motors regarding the target torque and current limitation," *Structural and Multidisciplinary Optimization*, vol. 64, no. 2, pp. 859–870, Aug. 2021, doi: 10.1007/s00158-021-02897-0.

BIOGRAPHIES OF AUTHORS



Mohd Zulsyazwan Allan was born in Sabah, Malaysia, in 1999. He received his Bachelor of Engineering degree in electrical engineering from Universiti Teknikal Malaysia Melaka (UTeM), Malaysia, in 2025. He is currently pursuing a Master of Science degree at the same university. He can be contacted at email: syazwanallan67@gmail.com.



Mohd Luqman Mohd Jamil received his Bachelor of Engineering degree from Universiti Teknologi MARA, Shah Alam, Malaysia, in 2000; his Master of Science degree from Newcastle University, Newcastle upon Tyne, United Kingdom, in 2003; and his Doctor of Philosophy degree from the University of Sheffield, Sheffield, United Kingdom, in 2011. All three degrees were in electrical engineering. He is currently an academic staff member at the Faculty of Electrical Technology and Engineering, Universiti Teknikal Malaysia Melaka, Melaka, Malaysia. His research interests include the design, analysis, and control of electric machines. He can be contacted at email: luqman@utem.edu.my.



Jenn Hwai Leong received his Doctor of Philosophy degree from the University of Sheffield, United Kingdom, in 2012. He is currently a member of the academic staff at the Faculty of Electrical Engineering Technology, Universiti Malaysia Perlis, Malaysia. His research interests include electric motors and drives. He can be contacted at email: jhleong@unimap.edu.my.